

Article

# A Performance Optimized CSTBT with Low Switching Loss

Hang Xu , Tianyang Feng, Wenrong Cui, Yafen Yang \*  and David Wei Zhang

School of Microelectronics, Fudan University, Shanghai 200433, China

\* Correspondence: yafen\_yang@fudan.edu.cn

**Abstract:** A novel Performance Optimized Carrier Stored Trench Gate Bipolar Transistor (CSTBT) with Low Switching Loss has been proposed. By applying a positive DC voltage to the shield gate, the carrier storage effect is enhanced, the hole blocking capability is improved and the conduction loss is reduced. The DC biased shield gate naturally forms inverse conduction channel to speed up turn-on period. Excess holes are conducted away from the device through the hole path to reduce turn-off loss ( $E_{\text{off}}$ ). In addition, other parameters including ON-state voltage ( $V_{\text{on}}$ ), blocking characteristic and short circuit performance are also improved. Simulation results demonstrate that our device exhibits a 35.1% and 35.9% decrease in  $E_{\text{off}}$  and turn-on loss ( $E_{\text{on}}$ ), respectively, in comparison with the conventional shield CSTBT (C<sub>on</sub>-SGCSTBT). Additionally, our device achieves a short-circuit duration time that is 2.48 times longer. In high-frequency switching applications, device power loss can be reduced by 35%. It should be noted that the additional DC voltage bias is equivalent to the output voltage of the driving circuit, enabling an effective and feasible approach towards high-performance power electronics applications.

**Keywords:** CSTBT; shield gate; DC bias; low switching loss; conduction loss

## 1. Introduction

Insulated Gate Bipolar Transistor (IGBT) is the core device in power electronic devices used for electric energy conversion and circuit control [1–3]. Various IGBT structures and techniques have been proposed and studied, including the field stop IGBT (FS-IGBT) [4], injection enhanced gate transistor (IEGT) [5] and carrier stored trench-gate bipolar transistor (CSTBT) [6]. With IGBT discrete devices and IGBT modules having an output power of up to 10 MW, they are widely utilized in high-voltage systems of Electric Vehicle, such as the main drive inverter, on-board charger (OBC), battery management system, on-board air conditioning control system, steering and other high-voltage auxiliary systems. In addition, IGBT is extensively employed in DC and AC charging piles, making them the cornerstone of the Electric Vehicle ecosystem.

For modern electronic systems represented by Electric Vehicles, higher operating frequency and higher power output are essential design goals. In the power converter system of Electric Vehicles (e.g., DC/DC converter, DC-to-DC inverter and the electronic power transformer), increasing the operating frequency can significantly benefit the system by reducing its volume, eliminating total harmonic distortion and improving power quality [7,8].

However, IGBT is still bottlenecked by technical and physical limitations, such as the unique trailing current and resulting switching loss that restrict the switching frequency to below 20 kHz [9–11]. Among the IGBTs mentioned above, CSTBT stands out as a promising candidate for the next-generation power electronics due to its ability to significantly reduce the on-state voltage while improving the carrier distribution in trench IGBT [12–14].

In a typical CSTBT, an additional carrier storage (CS) layer with a higher doping concentration is located between the P-type well region (P-body) and the N-drift region. In the on-state, the CS layer acts as a higher potential barrier that blocks holes from being collected by the emitter, leading to hole accumulation in the drift region near emitter side [15,16]. Accordingly,



**Citation:** Xu, H.; Feng, T.; Cui, W.; Yang, Y.; Zhang, D.W. A Performance Optimized CSTBT with Low Switching Loss. *Micromachines* **2023**, *14*, 1039. <https://doi.org/10.3390/mi14051039>

Academic Editor: Andrea N. Tallarico

Received: 25 April 2023

Revised: 6 May 2023

Accepted: 8 May 2023

Published: 12 May 2023



**Copyright:** © 2023 by the authors. Licensee MDPI, Basel, Switzerland. This article is an open access article distributed under the terms and conditions of the Creative Commons Attribution (CC BY) license (<https://creativecommons.org/licenses/by/4.0/>).

this causes a considerable number of electrons to be injected through the emitter, maintaining electrical neutrality and increasing the carrier concentration [17,18].

The switching frequency of optimized IGBTs is limited to 20 kHz to 40 kHz, which falls short of the desired 100 kHz, resulting in a tradeoff between high power and high frequency [19–21].

Therefore, improving the switching performance of IGBT has become a highly concerned issue, with two primary limiting factors listed below:

1. Inherent tail current affecting the switching performance.
2. Overheating caused by excessive switching loss, which is the main limiting factor at present [22].

Switching frequency refers to the number of times the IGBT is switched on and off within a second. Under the specified bus voltage and current, IGBT will generate power loss every time it switches. As the switching frequency increases, so does the power loss and temperature rise, which could lead to IGBT failure if the temperature exceeds the upper limit. The total power losses of an IGBT chip are typically composed of turn-on loss ( $E_{on}$ ), turn-off loss ( $E_{off}$ ) and conduction loss, and are proportional to the product of frequency and switching loss ( $E_{off} + E_{on}$ ).

In high frequency switching applications above 20 kHz, the reduction of switching loss becomes crucial, as it accounts for the majority of the total power consumption (above 60%), as shown in Figure 1b. In order to reduce the total power consumption under the switching frequency of 20~50 kHz, IGBT chip performance must be set at the position of high  $V_{on}$ , low  $E_{on}$  and  $E_{off}$ , like High speed IGBT in Figure 1a.

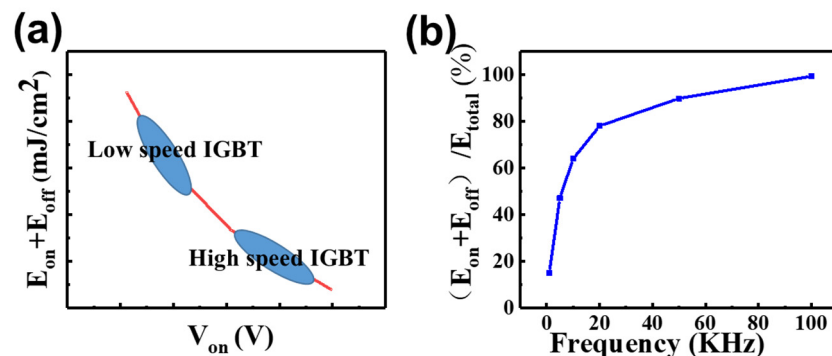


**Figure 1.** (a) Tradeoff relationship between  $V_{on} - (E_{off} + E_{on})$ . (b) The proportion of  $E_{off} + E_{on}$  in total power loss under different frequency (Calculated according to IGBT data sheet).

Currently, shield gate technology (SGT) is a promising way to reduce switching loss by decreasing  $Q_g$ . However, the grounded bottom electrode in SGT increases channel resistance, leading to a serious impact on  $V_{on}$  and a corresponding rise in conduction loss.

In this work, we propose a CSTBT device with a forward DC bias shield gate and hole path (DC-CSTBT). The characteristics of low  $V_{on}$ , low  $E_{on}$ , low  $E_{off}$  and high breakdown voltage are demonstrated simultaneously. The proposed device only made minor changes on the basis of conventional CSTBT and offers a simple and easy-to-implement structure and process.

## 2. Structure and Process Flow

The schematic diagram of the proposed DC-CSTBT is shown in Figure 2a. Compared with the conventional CSTBT shown in Figure 2b, both devices have the same doping profile except for an extra N-type carrier storage layer (CS2).

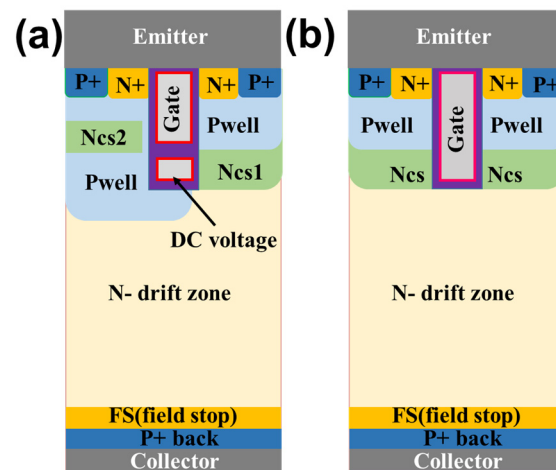


**Figure 2.** (a) The proposed DC-CSTBT; (b) Conventional CSTBT.

In the proposed DC-CSTBT, the trench gate is split into two parts, including the upper and deeper parts. The upper part is connected to the gate control signal, controlling the turning on and off of the device. The deeper shield trench gate is connected to a positive DC bias. Generally, the DC bias value is the same as the gate saturation turn-on voltage, and there is no need to add the additional output of the driving circuit.

The CS2 region on the left is achieved by additional lithography and ion implantation. There is a gap between the trench and the CS2, and the state (on/off) of this hole path is completely controlled by the trench gate voltage. In the on state, the hole channel is closed, and the gap is inverted and acts as a whole CS storage layer with a CS2 layer. As the CS2 locates away from the bottom of the trench, its doping concentration is high to reduce  $V_{on}$  without blocking characteristic deterioration. Table 1 shows the major structural parameters of the proposed device.

**Table 1.** Major structural parameters.

Parameter	Value
Cell pitch	4 $\mu\text{m}$
Gate oxide thickness	120 nm
N-drift doping	$5.9 \times 10^{13} \text{ cm}^{-3}$
CS doping	$4.0 \times 10^{14} \text{ cm}^{-3}$
High doping CS (CS2)	$1.5 \times 10^{17} \text{ cm}^{-3}$
P-well doping	$3.0 \times 10^{16} \text{ cm}^{-3}$
Trench depth	5 $\mu\text{m}$

The split trench gate technology is compatible with the current manufacturing process. The process flow of the device is shown in Figure 3. The main process steps include epitaxial layer formation, ion implantation, trench etching, polysilicon deposition and etching, oxide layer formation, etc. Two additional processes compared with the conventional CSTBT process are highlighted in red, namely the polysilicon etching and the oxide layer deposition.

In addition, the detailed device process of split gate formation is shown in Figure 4a–f below. After deep trench etching (Figure 4a), an oxide (Figure 4b) and a very thick polysilicon (Figure 4c) is deposited in the trench. Then, part of the polysilicon is etched (Figure 4d), and only the bottom part as a shield gate is left. Subsequently, an oxide layer is deposited to complete the isolation of the upper and lower split gates (Figure 4e). Finally, polysilicon is deposited into the trench to form the split gate (Figure 4f). The split gate at the bottom serves as the DC bias shielding gate in the paper. Figure 4g shows the formation of CS2 on the left. A high-energy ion injection is added after an emitter injection, and the distribution of the CS2 layer is defined by mask.

- CS layer Ion IMP
- Deep trench etching
- Poly deposition
- Poly etching
- Oxide deposition
- Poly deposition and CMP
- Emitter and CS2 Ion IMP
- Deposit metal and surface CMP
- Back collector Ion IMP
- Back metallization

Figure 3. Process flow diagram. IMP (Ion implantation) CMP (Chemical mechanical polishing). Two additional processes are highlighted in red.

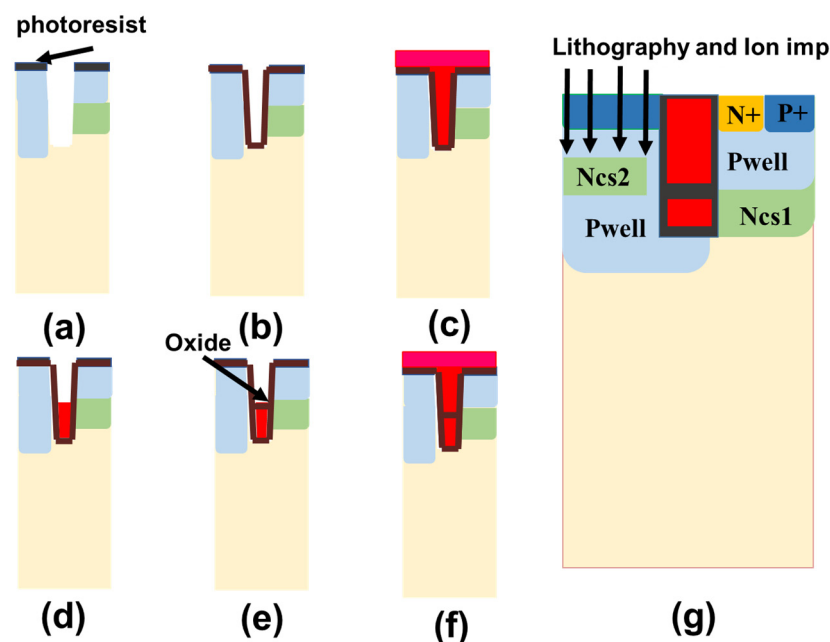


Figure 4. The formation process of DC bias shielding gate and extra CS2 in the proposed device. (a) deep trench etching. (b) oxide deposition. (c) polysilicon deposition. (d) polysilicon etching. (e) oxide deposition to complete the isolation. (f) polysilicon deposition to form the split gate. (g) the formation of CS2.

Despite the slight increase in device fabrication complexity or cost associated with the proposed DC bias shielding approach, the process steps are completely consistent with those of existing trench IGBT devices. Additionally, the inclusion of a DC bias shield gate necessitates only minimal alterations to the driving circuit and requires the addition of only one lithography mask. This device has a simple structure and low cost, with great potential for practical applications.

### 3. Simulation Results and Discussion

The device model is established by the Sentaurus Technology Computer-Aided Design (TCAD) simulation, and the process conditions are based on the SMIC 0.18  $\mu\text{m}$  process node. The following four aspects of optimization brought by DC bias shielding are introduced. The structures contrasted below include a conventional CSTBT, a conventional shield CSTBT with a grounded shield gate ( $C_{\text{on-SGCSTBT}}$ ), DC-CSTBT, referring to CSTBT without a split gate, a split gate CSTBT with grounded shield gate and the proposed DC bias CSTBT, respectively.

A. Low  $E_{on}$

There are two factors contributing to the low  $E_{on}$ . Firstly, the SGT gate structure reduces the Miller capacitance, which helps to decrease the  $E_{on}$ . The Miller effect induces the formation of a platform voltage when driving the trench gate, which subsequently prolongs switching time and heightens switching loss. These consequences can have profoundly detrimental effects on the normal operation of the IGBT. Secondly, the shield gate DC bias technology accelerates the formation of conductive channels, further reducing the  $E_{on}$ .

(1) low  $Q_{GC}$

In the conventional CSTBT structure, the whole  $C_{GC}$  is composed of three parts, as depicted in Figure 5c; namely,  $C_{GC1}$ ,  $C_{GC2}$  and  $C_{GC3}$ .  $C_{GC1}$  and  $C_{GC2}$  are mainly related to gate oxide thickness and the coupling area between trench and collector. Among these three parts,  $C_{GC3}$  is the most dominant factor. Compared with a conventional CSTBT, the deeper trench of the proposed device is DC biased (equivalent to AC ground), resulting in a smaller coupling area between the gate and collector. The charging time of the Miller capacitor is reduced by 42.7% in the proposed DC-CSTBT compared with the conventional CSTBT.  $Q_{GC}$  is reduced from 61.3 nC to 35.1 nC, and the Miller capacitance of the proposed device, equivalently, is decreased from 8.636 nF/cm<sup>2</sup> to 2.57 nF/cm<sup>2</sup>. The reduction in Miller capacitance is mainly transformed into  $C_{GE}$ . The simulation results indicate that the  $Q_{GC}$  of the proposed device remains constant under a different DC bias, as depicted in Figure 5b. Therefore, a higher DC bias can enhance the carrier storage effect without deteriorating the Miller effect.

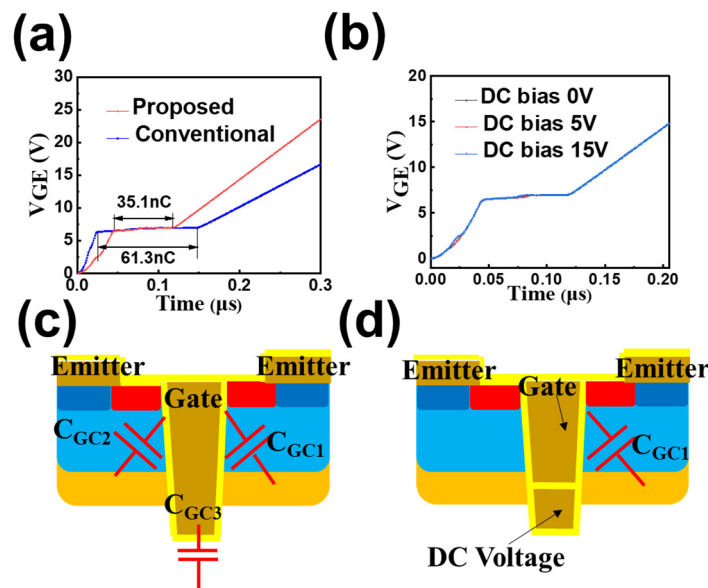


**Figure 5.** (a) Gate charge curve for conventional CSTBT and the proposed DC-CSTBT. (b) Gate charge curve of the proposed device under different DC bias. (c) Main distribution of  $C_{GC}$  in conventional device. (d) Main distribution of  $C_{GC}$  in the proposed device.

(2) Faster turn-on by forward biased bottom inversion channel

$C_{on}$ -SGCSTBT will bring the problem of excessive  $V_{on}$ . To address this, the improved DC-CSTBT is proposed here.

Figure 6 shows the turn-on curve of the proposed device under a clamped load. The collector current voltage and collector current of the proposed device is swifter than  $C_{on}$ -SGCSTBT, as depicted in Figure 6a,b. This improvement can be attributed to the inverse channel forward formed by the DC voltage at the trench bottom rather than the grounded deep trench. The formation of a conductive channel is accelerated and the turn-on process is sped up effectively by the DC biasing technique.

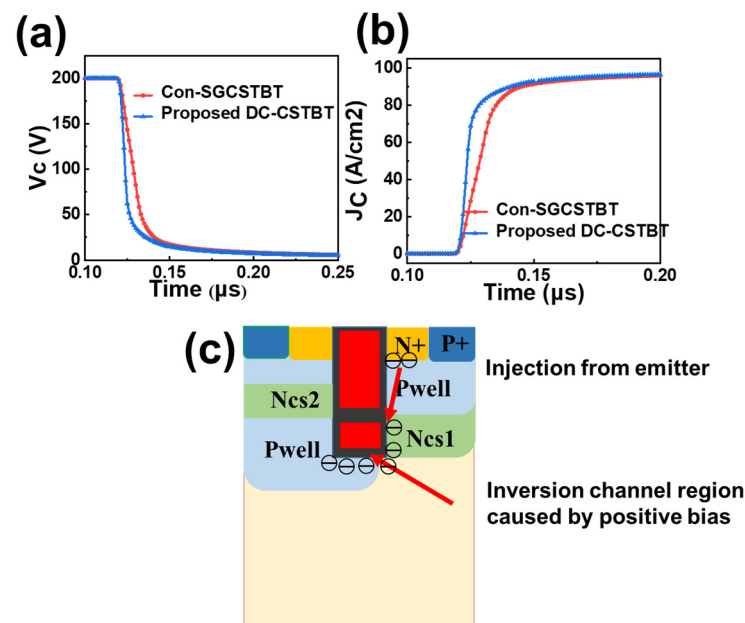


**Figure 6.** Turn-on curve (a)  $V_c$  curve during turn-on process; (b)  $J_c$  curve during turn-on process; (c) Working mechanism of DC voltage bias shield gate.

The turn-on process of the IGBT is as follows. First, a positive bias is applied at the trench, which inverts the P-base region to form an N channel. Then, the emitter releases electrons into the drift region through this channel, leading to the potential drop in the drift region. When the potential is low to a certain threshold, the collector PN junction conducts forward, and holes are injected into the N-region; conductance modulation effect starts.

Figure 7 shows the distribution of electron current during the turn-on state. Large electron currents flowing to the drift region can be clearly seen at the trench bottom. The mechanism can be explained as follows. There exists a DC bias at the shield gate and a corresponding electric field pointing from the trench bottom to the emitter. Consequently, electrons in the emitter are injected through the inversion layer around the shield gate, resulting in a decrease in the N-drift potential.

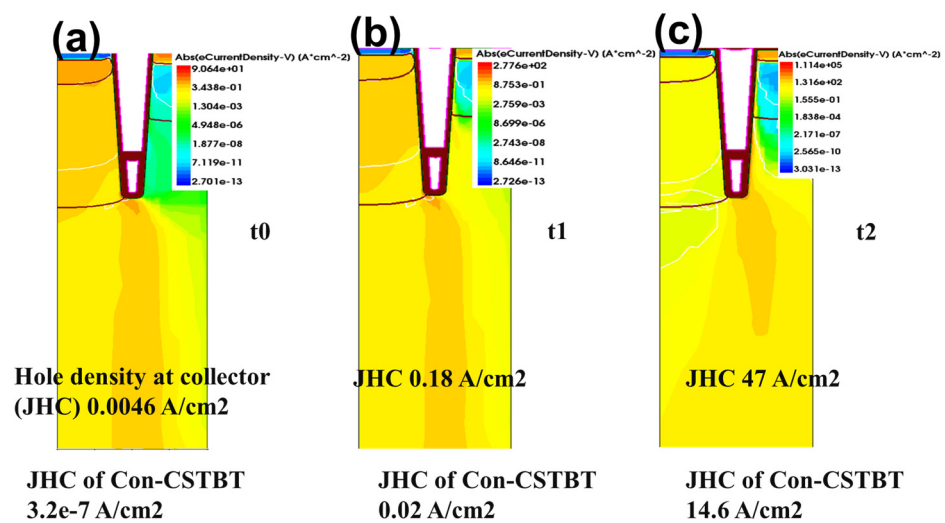


**Figure 7.** Electron current distribution during turn-on process of the proposed DC-CSTBT with 15 V DC bias (a) at  $t_0$ ; (b) at  $t_1$ ; (c) at  $t_2$ ; ( $t_0$   $t_1$   $t_2$  three moments are after turn-on at  $1 \times 10^{-7}$  ns,  $2 \times 10^{-7}$  ns,  $3 \times 10^{-7}$  ns, respectively).

Moreover, the hole current density at the collector region is marked, which can further compare the collector injection speed, as illustrated in Figure 7a–c. At  $t_0$ , the hole current

density at the collector ( $J_{CH}$ ) of DC-CSTBT is  $10^4$  larger than that of the normal grounded shield gate. At  $t_1$ ,  $J_{CH}$  of DC-CSTBT is also nine times larger. Until  $t_2$ , both reach an order of magnitude of  $47 \text{ A/cm}^2$  and  $14.6 \text{ A/cm}^2$ , respectively. It is further proved that the DC bias shield can speed up the device turn-on process.

Figure 8 shows the turn-on curve of the proposed DC-CSTBT (under various DC bias). It can be seen that the  $J_C$  of the DC-CSTBT with a higher DC voltage is much swifter. A higher DC bias contributes to a stronger electric field to promote the incident of electrons. In addition, during the turn-on process,  $dV/dt$  and  $dI/dt$  are significantly improved, and the turn-on loss can be reduced. The simulation results show that, compared with the  $C_{on}$ -SGCSTBT, the  $E_{on}$  of the proposed device can be reduced by 35.9%, from  $3.2 \text{ mJ/cm}^2$  to  $2.05 \text{ mJ/cm}^2$ .

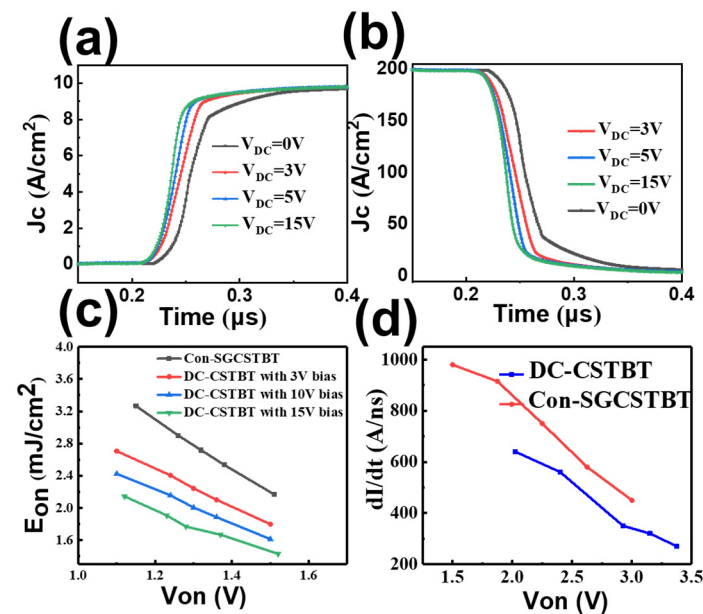


**Figure 8.** (a)  $J_c$  curve during turn-on process under different DC bias; (b)  $V_c$  curve during turn-on process; (c) Trade off relationship between  $E_{on}$  and  $V_{on}$  in the proposed DC-CSTBT and  $C_{on}$ -SGCSTBT. (d)  $V_{on}$  versus  $dI/dt$  of the proposed DC-CSTBT and  $C_{on}$ -SGCSTBT in turn-on process.

### B. Low $E_{off}$

Figure 9a illustrates the transient hole current distribution during the turn-off at  $t_1$  (a period of time after the turn on time  $t_0$ ) of the DC-CSTBT and hole current values along  $C_1$ . It can be seen that the highest hole current is concentrated at the designed hole path, reaching more than  $1 \times 10^4 \text{ A/cm}^2$  as depicted in Figure 9b.

In the turn-off process, the inversed hole path recovers into the P-region with  $V_G$  transferring to zero. Consequently, the accumulated holes in the drift region are swept out through the inversion layer around the hole path region, accelerating hole extraction to make the drift zone reach neutrality as soon as possible.

The mixed-mode, clamped, inductive switching simulation is performed to study the turn-off performance. The simulated devices are set to the same current of 10 A at the current density of  $100 \text{ A/cm}^2$ . The DC bus voltage ( $V_{bus}$ ) is set to 1500 V. The load inductance  $L_c$  load is 1 mH and the circuit is shown in Figure 10a. The gate voltage decreases from 15 to 0 V to turn off the device. The simulated turn-off process of  $C_{on}$ -SGCSTBT and the proposed DC-CSTBT (with same  $V_{on}$  of 1.5 V) are shown in Figure 10b,c. Clearly, the  $T_{off}$  of the DC-CSTBT is much smaller than that of  $C_{on}$ -SGCSTBT, which indicates that the  $E_{off}$  of the proposed device is more excellent.

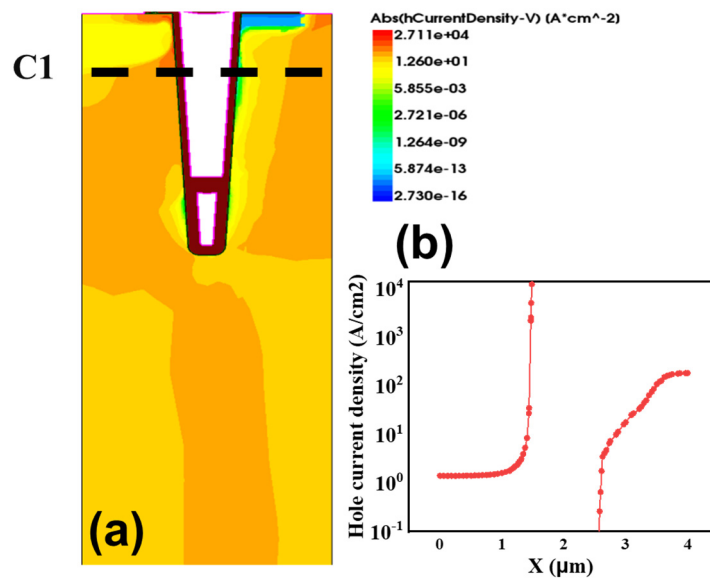


Figure 9. Transient hole current distribution during turn-off (a) curve during turn-off process at  $t_1$  (a period of time after the turn off time  $t_0$ ); (b) hole current value along C1 at  $t_1$ .

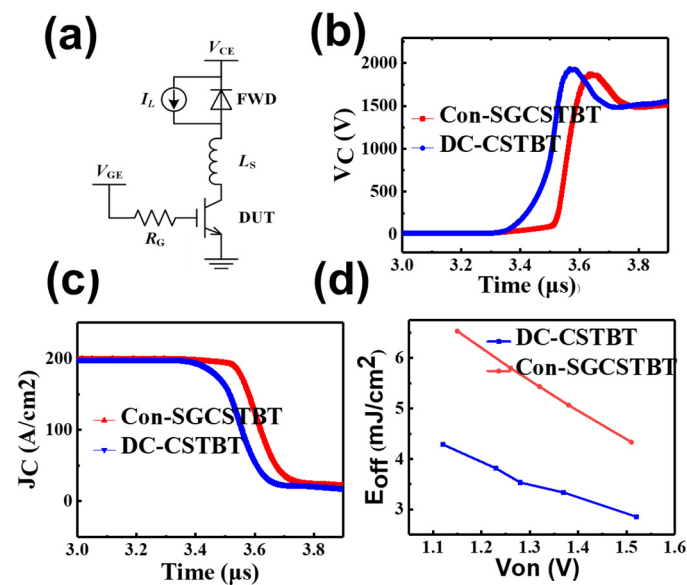
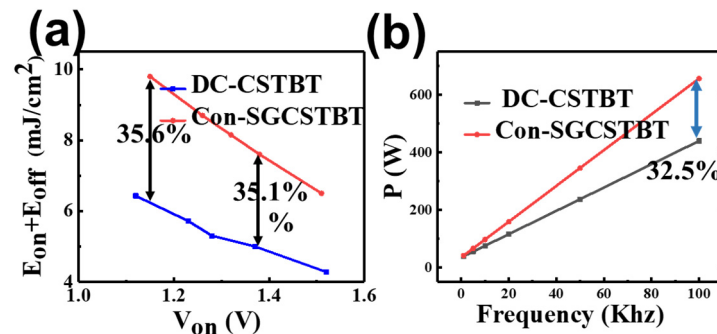


Figure 10. (a) Circuit schematic for turn-off transient analysis. ( $V_{cc} = 1750\text{ V}$   $L_c = 1\text{ mH}$   $L_s = 1.5\text{ fH}$   $R_g = 10\ \Omega$ ). (b) Turn off waveform of collector voltage. (c) Turn off waveform of collector current. (d) Trade off relationship between  $E_{off}$  and  $V_{on}$  in the proposed DC-CSTBT and  $C_{on}$ -SGCSTBT.

Figure 10d illustrates the relationship between  $E_{off}$  and  $V_{on}$  for the two different structures, after changing the peak P-collector doping concentration. Under  $V_{on} = 1.15\text{ V}$ , the  $E_{off}$  of the proposed DC-CSTBT is  $6.5\text{ mJ/cm}^2$ , which is 36.1% lower than that of the  $C_{on}$ -SGCSTBT ( $4.15\text{ mJ/cm}^2$ ). In addition, the switching loss, including  $E_{on}$  and  $E_{off}$ , are further compared, as shown below.

Figure 11 shows the tradeoff curves of  $V_{on} - (E_{off} + E_{on})$  for the devices. It is observed that the tradeoff curves of DC-CSTBT is obviously more optimized than  $C_{on}$ -SGCSTBT. This is mainly due to the presence of both a hole path and emitter electron injection acceleration techniques, which improve turn-on and turn-off, respectively. For the same  $V_{on}$  1.38 V,  $E_{off} + E_{on}$  of DC-CSTBT is decreased by 35.1% compared with the  $C_{on}$ -SGCSTBT. However, with the  $V_{on}$  of 1.14 V, this reduction percentage is still higher. Considering the same  $E_{off} + E_{on}$  of  $6.4\text{ mJ/cm}^2$ , the  $V_{on}$  of the DC-CSTBT can be 25.8% lower than that of the

$C_{on}$ -SGCSTBT. Therefore, DC-CSTBT have a better tradeoff between  $V_{on}$  and  $E_{off} + E_{on}$  than  $C_{on}$ -SGCSTBT. Correspondingly, the calculated power loss in high-frequency switching applications (100 kHz) can be reduced by 32.5% as shown in Figure 11b.



**Figure 11.** (a) Trade off relationship between  $V_{on} - (E_{off} + E_{on})$ . (b) Relationship between power loss and switching frequency.

### C. Blocking characteristics

As mentioned above, the breakdown voltage of the trench IGBT is affected by the deep trench structure. The breakdown voltage of the trench IGBT is lower than that of the traditional planar type because of the pre-breakdown of trench bottom.

Especially with the introduction of the carrier enhancement layer, the electric field at the bottom becomes too concentrated. The reason for the high electric field is the largest potential difference at the trench bottom. The electric potential of the trench is 0 V, which is the lowest potential at the same depth in the drift region. Breakdown initially occurs at the bottom of the trench. Some structures have previously been proposed to attenuate the overly concentrated electric field, such as implanting the P-type doped well at the bottom. However, the conduction loss will increase significantly because of the drift zone resistance increase. To address this issue, the proposed DC bias device employs a deeper trench electrode connected with a forward DC bias to reduce the potential difference at the bottom trench by raising the potential at the shield gate, thus relieving the electric field at the bottom of the trench effectively. Figure 12a,b show the impact ionization distribution under same reverse bias at 1800 V. It should be noted that  $C_{on}$ -SGCSTBT shows similar breakdown characteristics as a conventional CSTBT for the same electric field distribution at the trench bottom, while the proposed device can reduce the peak impact by about 50% compared with  $C_{on}$ -SGCSTBT.

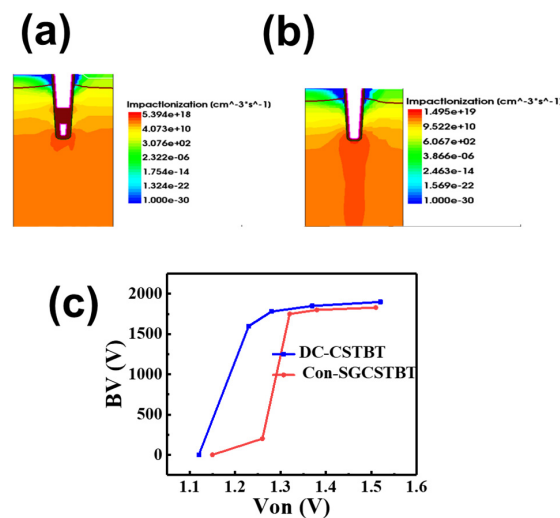


**Figure 12.** (a) Impact ionization rate of DC-CSTBT under 1800 V reverse bias. (b) Impact ionization rate of conventional CSTBT under 1800 V reverse bias. (c) Dependence of the breakdown voltage and varying  $V_{on}$ .

Figure 12c illustrates the tradeoff relationship between BV and  $V_{on}$  of  $C_{on}$ -SGCSTBT and the proposed DC-CSTBT (by changing the doping concentration of the CS layer). Under the same  $V_{on}$ , the proposed device always has a higher BV because of the weakened electric field at the trench bottom. For  $C_{on}$ -SGCSTBT, the BV starts to decrease when  $V_{on}$  is smaller than 1.35 V (reduce the conduction pressure drop by increasing the concentration of CS). While the proposed device can maintain 1600 V withstand voltage until  $V_{on}$  is smaller than 1.2 V. The present device achieves a better tradeoff relationship.

#### D. Conduction characteristics

The forward DC bias at the deep shield trench repels positively charged holes because of mutual repulsion between positive charges, promoting the accumulation of holes near the trench bottom, as depicted in Figure 13a. Therefore, a large number of holes accumulates at the emitter side. In order to maintain electrical neutrality, the emitter should emit a corresponding quantity of electrons. With the increase in carrier doping concentrations in the drift region, the on-resistance of the device is reduced. Figure 13b shows the comparison of output characteristics of the proposed device under different forward DC voltages including 0 V, 3 V and 15 V. It is clear that  $V_{on}$  decreases with DC bias rises, as a higher DC voltage contributes to a stronger hole block effect. Figure 13c compares the distributions of the hole carrier density along line C2 for DC-CSTBT and with a DC bias at collector current density  $J = 100 \text{ A/cm}^2$ . As the DC bias at the deeper electrode only contributes to a higher hole carrier density near the emitter, only a little penalty in the switching losses will be added.

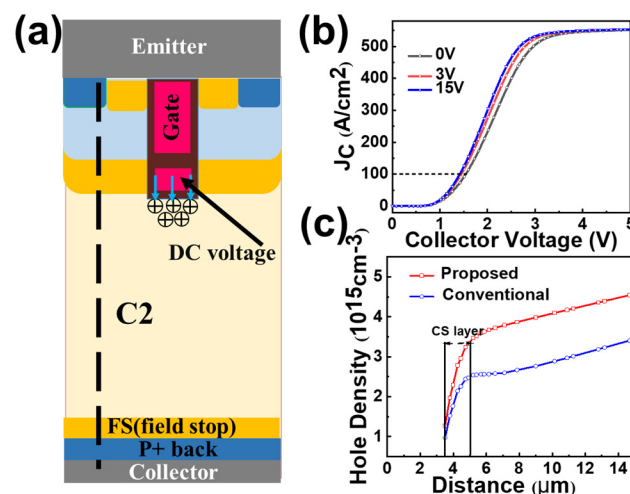
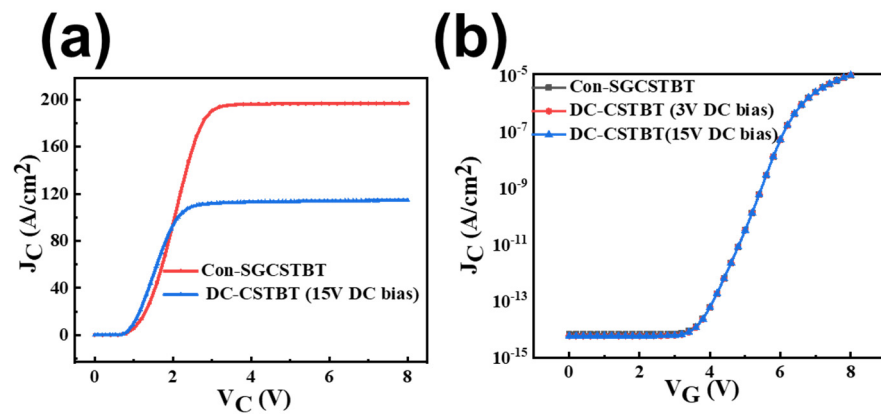


**Figure 13.** (a) Schematic diagram of carrier storage effect enhancement mechanism. (b)  $I_D$ - $V_D$  curves of DC-CSTBT under different DC bias. (c) Distributions of the hole carrier density along line C2 shown in at collector current density  $J = 100 \text{ A/cm}^2$ .

#### E. Other characteristics

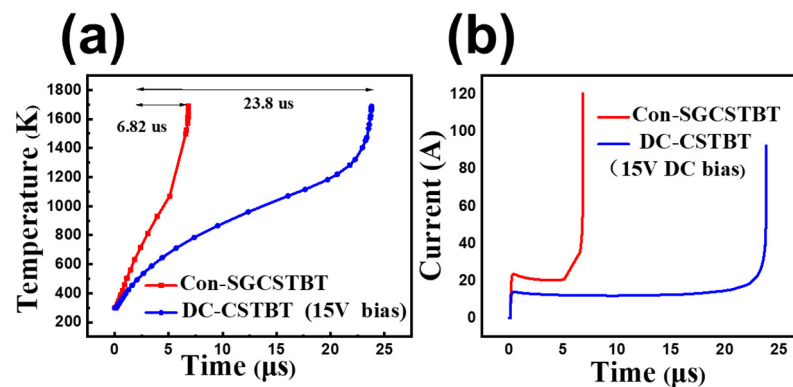
Output characteristics, transfer characteristics and short circuit characteristics are also studied. Simulation results show that the  $J_C$ - $V_G$  curve does not change, while the saturation current and short circuit characteristics are greatly optimized.

Figure 14a shows that the saturation current density is significantly reduced compared with  $C_{on}$ -SGCSTBT, since no current flows through the left half of the proposed DC-CSTBT. In addition, Figure 14b shows the transfer characteristics ( $J_C$ - $V_G$  curve) of  $C_{on}$ -SGCSTBT and the proposed device under the same  $V_{on}$ . The curve of both devices almost overlap, indicating that the proposed structure only optimizes the device characteristics by adding a DC bias shield structure, while preserving the basic transfer characteristics of the device.



**Figure 14.** (a) Output characteristics of  $C_{on}$ -SGCSTBT and DC-CSTBT. (b) Transfer characteristics of  $C_{on}$ -SGCSTBT and DC-CSTBT.

Figure 15 shows short-circuit waves. It indicates that the DC-CSTBT withstands a significantly longer short-circuit duration time (device failure time is defined when lattice temperature reaches 1687 K) than that of the  $C_{on}$ -SGCSTBT before failure. Owing to the smaller saturation current density, the short-circuit time of the proposed DC-CSTBT structure is about 2.48 times longer than that of the  $C_{on}$ -SGCSTBT.



**Figure 15.** (a) Maximum device temperature curves in the short-circuit situation of the two devices. The self-heating effect is considered by the LAT.TEMP model with the initial device temperature of 300 K. (b) Simulated short-circuit current of the  $C_{on}$ -SGCSTBT and the proposed DC-CSTBT devices.

#### 4. Conclusions

A novel DC-CSTBT with additional forward DC bias is proposed and investigated by numerical simulations. The trench is split into two parts, the upper one serves as a normal gate electrode while the deeper one is biased by forward DC voltage to block holes from flowing to the emitter. By combining the enhanced carrier storage effect caused by forward bias and hole path, the proposed device shows excellent performance. Specifically, the new structure exhibits a 42.7% decrease in  $Q_{GC}$ ;  $E_{off}$  and  $E_{on}$  are reduced by 35.1% and 35.9%. Importantly, the process steps are completely consistent with the existing trench IGBT devices. Only two simple process steps are added, and only one additional lithography mask is needed, making the device highly practical with the potential for low cost and a simple structure.

**Author Contributions:** Writing—original draft, H.X. and Y.Y.; validation, T.F.; software, W.C.; supervision, D.W.Z. All authors have read and agreed to the published version of the manuscript.

**Funding:** This work was supported by the Science and Technology Commission of Shanghai Municipality (21DZ1100700).

**Data Availability Statement:** Not applicable.

**Conflicts of Interest:** The authors declare no conflict of interest.

## References

1. Laska, T.; Munzer, M.; Pfirsch, F.; Scaeffler, C.; Schmidt, T. The field stop IGBT (FS IGBT). A new power device concept with a great improvement potential. In Proceedings of the 12th International Symposium on Power Semiconductor Devices & ICs, Toulouse, France, 22–25 May 2000; pp. 355–358. [[CrossRef](#)]
2. Kitagawa, M.; Omura, I.; Hasegawa, S.; Inoue, T.; Nakagawa, A. A 4500 V injection enhanced insulated gate bipolar transistor (IEGT) operating in a mode similar to a thyristor. In Proceedings of the IEEE International Electron Devices Meeting, Washington, DC, USA, 5–8 December 1993; pp. 679–682. [[CrossRef](#)]
3. Takahashi, H.; Haruguchi, E.; Hagino, H.; Yamada, T. Carrier stored trench-gate bipolar transistor (CSTBT)—A novel power device for high voltage application. In Proceedings of the 8th International Symposium on Power Semiconductor Devices and ICs, Maui, HI, USA, 23–23 May 1996; pp. 349–352. [[CrossRef](#)]
4. Hshieh, F.-I. Double Gate-Oxide for Reducing Gate-Drain Capacitance in Trenched DMOS with High-Dopant Concentration Buried-Region under Trenched Gate. U.S. Patent 6 262 453, 17 July 2001.
5. Jiang, Q.; Wang, M.; Chen, X. A high-speed deep-trench MOSFET with a self-biased split gate. *IEEE Trans. Electron Devices* **2010**, *57*, 1972–1977. [[CrossRef](#)]
6. Antoniou, M.; Lophitis, N.; Bauer, F.; Nistor, I.; Bellini, M.; Rahimo, M.; Amaratunga, G.; Udrea, F. Novel approach toward plasma enhancement in trench-insulated gate bipolar transistors. *IEEE Electron Device* **2015**, *36*, 823–825. [[CrossRef](#)]
7. Williams, R.K.; Darwish, M.N.; Blanchard, R.A.; Siemieniec, R.; Rutter, P.; Kawaguchi, Y. The Trench Power MOSFET: Part I—History, Technology, and Prospects. *IEEE Trans. Electron Devices* **2017**, *64*, 674–691. [[CrossRef](#)]
8. Huang, J.; Huang, H.; Lyu, X.; Chen, X.B. Simulation Study of a Low Switching Loss FD-IGBT With High  $dI/dt$  and  $dV/dt$  Controllability. *IEEE Trans. Electron Devices* **2018**, *65*, 5545–5548. [[CrossRef](#)]
9. Huang, J.; Huang, H.; Chen, X.B. Simulation Study of a Low ON-State Voltage Superjunction IGBT With Self-Biased PMOS. *Trans. Electron Devices* **2019**, *66*, 3242–3246. [[CrossRef](#)]
10. Jiang, M.; Gao, L. Simulation Study of a Thyristor Conduction-Insulated Gate Bipolar Transistor (TC-IGBT) With a p-n-p Base and an n-p-n Collector for Reducing Turn-Off Loss. *IEEE Trans. Electron Devices* **2020**, *67*, 2854–2858. [[CrossRef](#)]
11. Ding, Y.; Yang, X.; Liu, G.; Wang, J. Physics-Based Trench-Gate Field-Stop IGBT Modeling with Optimization-Based Parameter Extraction for Device Parameters. *IEEE Trans. Electron Devices* **2021**, *68*, 6305–6312. [[CrossRef](#)]
12. Saito, W.; Nishizawa, S. Alternated Trench-Gate IGBT for Low Loss and Suppressing Negative Gate Capacitance. *IEEE Trans. Electron Devices* **2020**, *67*, 3285–3290. [[CrossRef](#)]
13. Chen, W.; Cheng, J.; Huang, H.; Zhang, B.; Chen, X.B. The Oppositely Doped Islands IGBT Achieving Ultralow Turn Off Loss. *IEEE Trans. Electron Devices* **2019**, *66*, 3690–3693. [[CrossRef](#)]
14. Zhang, J.; Wang, K.; Luo, J.; Zhao, Y.; Li, Z.; Ren, M.; Gao, W.; Zhang, B. Numerical analysis of impact of shield gate on trench IGBT and CSTBT. In Proceedings of the IEEE International Conference on Electron Devices and Solid-State Circuits, Xi'an, China, 12–14 June 2019; pp. 1–3.
15. Xu, H.; Yang, Y.; Tan, J.; Zhu, H.; Sun, Q.Q.; Zhang, D.W. Carrier Stored Trench-Gate Bipolar Transistor With Stepped Split Trench-Gate Structure. *IEEE Trans. Electron Devices* **2022**, *69*, 5450–5455. [[CrossRef](#)]
16. Sawada, M.; Ohi, K.; Ikura, Y.; Onozawa, Y.; Otsuki, M.; Nabetani, Y. Trench shielded gate concept for improved switching performance with the low miller capacitance. In Proceedings of the 2016 28th International Symposium on Power Semiconductor Devices and ICs (ISPSD), Prague, Czech Republic, 12–16 June 2016; pp. 207–210. [[CrossRef](#)]
17. Nishi, K.; Narazaki, A. CSTBT™ based Split-Gate RC-IGBT with Low Loss and EMI Noise. In Proceedings of the 2020 32nd International Symposium on Power Semiconductor Devices and ICs (ISPSD), Vienna, Austria, 13–18 September 2020; pp. 138–141. [[CrossRef](#)]
18. Luo, X.; Zhang, S.; Wei, J.; Yang, Y.; Su, W.; Fan, D.; Li, C.; Li, Z.; Zhang, B. A Low Loss and On-State Voltage Superjunction IGBT with Depletion Trench. In Proceedings of the 2020 32nd International Symposium on Power Semiconductor Devices and ICs (ISPSD), Vienna, Austria, 13–18 September 2020; pp. 130–133. [[CrossRef](#)]
19. Ortiz, G.; Uemura, H.; Bortis, D.; Kolar, J.W.; Apeldoorn, O. Modeling of Soft-Switching Losses of IGBTs in High-Power High-Efficiency Dual-Active-Bridge DC/DC Converters. *IEEE Trans. Electron Devices* **2013**, *60*, 587–597. [[CrossRef](#)]
20. Dujic, D.; Steinke, G.K.; Bellini, M.; Rahimo, M.; Storasta, L.; Steinke, J.K. Characterization of 6.5 kV IGBTs for High-Power Medium-Frequency Soft-Switched Applications. *IEEE Trans. Power Electron.* **2014**, *29*, 906–919. [[CrossRef](#)]
21. Fujita, S.; Hussein, K.H.; Kitamura, S.; Yamaguchi, T. Investigation on IGBT High-Frequency Plasma Extraction Transient Time Oscillation. *IEEE Trans. Power Electron.* **2009**, *24*, 1570–1576. [[CrossRef](#)]
22. Sheng, K.; Finney, S.J.; Williams, B.W. Thermal stability of IGBT high-frequency operation. *IEEE Trans. Ind. Electron.* **2000**, *47*, 9–16. [[CrossRef](#)]

**Disclaimer/Publisher’s Note:** The statements, opinions and data contained in all publications are solely those of the individual author(s) and contributor(s) and not of MDPI and/or the editor(s). MDPI and/or the editor(s) disclaim responsibility for any injury to people or property resulting from any ideas, methods, instructions or products referred to in the content.